CIMAC CONGRESS 25
ZURICH, MAY 19 – 23, 2025

2025 | 057

Sensitivity of modern in-cylinder pressure measurement and analysis to ammonia/hydrogen fuel blends

Basic research & advanced engineering - new concepts

David Rogers, Kistler Instrumente AG

Alasdair Cairns, University of Nottingham
Sikai Geng, Univeristy of Nottingham
Ajith Ambalakatte, Univeristy of Nottingham
David Mauke, Kistler Instrumente AG
Jonathan Hall, MAHLE Powertrain Ltd.
Mike Bassett, MAHLE Powertrain Ltd.
Anthony Harrington, MAHLE Powertrain Ltd.

ABSTRACT

Ammonia, as a carbon-free and effective hydrogen carrier, is a promising candidate as a feasible fuel for heavy-duty internal combustion engines to facilitate net zero. The aim of the currently reported work was to evaluate the sensitivity of in-cylinder pressure measurement and conventional analysis techniques to ammonia and hydrogen fuel blends. The work was undertaken using a modern single-cylinder spark ignition research engine equipped with independent variable valve timing, central coil-on-plug ignition, high tumble port design, separated ammonia and hydrogen port fuel injection, gasoline direct injection and an external boost rig. Engine testing was undertaken across a wide range of operating conditions covering varied engine speed, load, boost levels, air-to-fuel ratio and fuel blend ratio with optimized spark timing. The fuel-blend-ratio was also varied from pure hydrogen to pure ammonia where viable. The testing was undertaken using a Kistler KiBox2 system for real-time high-speed indication measurements of in-cylinder, intake port and exhaust port pressure. In-depth analysis involved parametric assessment of the sources of inaccuracy in current commonly adopted reverse mode heat release analysis routines covering key factors such as polytropic index, ignition delay, start of combustion, end of combustion, mass fraction burned and combustion phasing. With ammonia hydrogen co-combustion, although the maximum and minimum polytropic indices differ by up to 0.04 under varying hydrogen levels up to 50% and excess air ratios, the index during compression was found to reduce by up to 3.1% from default index of 1.32 for stoichiometric gasoline operations, which could lead to significant discrepancies in heat release calculations and compromise consistent combustion phasing control. Overall the work has provided detailed insight into the specific requirements of accurate pressure measurement with new hydrogen and ammonia fuel blends and has enabled improved precision during testing and post-processing. The insights gained on polytropic indices for different hydrogen ammonia operating conditions in this work will guide further analysis to determination of related Wiebe function “shape factors”, with direct comparisons made with conventional gasoline operation.

1 INTRODUCTION

Precise in-cylinder pressure measurement is essential for understanding and quantification of combustion in Internal Combustion (IC) engines, enabling assessment of essential metrics such as mass fraction burned profiles, combustion phasing and duration [1, 2]. Numerous studies have established best practices to mitigate sensor-induced measurement errors, including piezoelectric pressure sensor offset "pegging" (zero-level correction) [2, 3], thermal shock compensation [2-4] and dynamic post-processing routines to ensure data fidelity [5-7]. Amongst others, early work by Randolph [8-10], Brunt. [1-4] and Amann [11, 12] identified the inherent sensitivity of single-zone Heat Release Rate (HRR) calculations to sensor installation, polytropic indexing and in-cylinder pressure pegging strategies. More recent publications [5, 7, 13-16] have refined these methodologies for modern engines, highlighting the continued importance of transducer data quality in realising high engine efficiency and low pollutant emissions.

Despite progress in developing accurate real-time calculations of combustion metrics, rapidly growing interest in sustainable fuels, particularly non-hydrocarbon alternatives such as ammonia (NH_3) and hydrogen (H_2), introduce distinct challenges for pressure-based combustion analysis. Table 1 shows the key combustion characteristics of ammonia and hydrogen compared to gasoline. Ammonia incurs relatively favourable volumetric energy density as an effective hydrogen carrier for heavy-duty engines. However, it has a comparatively lower specific heat ratio, resulting in slower pressure and temperature buildup during compression. Furthermore, these two gases exhibit opposing combustion characteristics: [17, 18] Ammonia requires high ignition energy and has an extremely low burning velocity, while hydrogen exhibits the opposite behaviour. These differences impact key cycle parameters such as heat transfer, ignition delay and overall indicated thermal efficiency. Even well-established polytropic routines for compression and expansion strokes can yield inaccurate burn rate or phasing predictions if the polytropic index (n) deviates from typical gasoline/diesel values [16, 19]. Heat transfer, blow-by, and chemical kinetics also contribute to variability in n, leading to errors in established HRR calculations.

Table 1. Key combustion characteristics of ammonia, hydrogen and gasoline [20-25]

Species	**Hydrogen**		**Gasoline**
Formula	H_2	NH_3	C_xH_y
LHV (MJ/kg)	120	18.8	44.5
Laminar Burning Velocity @ λ=1 (m/s)	3.51	0.07	0.58
Auto-ignition Temperature (K)	773-850	930	503
Research Octane Number	>100	130	90-98
Flammability Limit in Air (vol.%)	4.7-75	15-28	0.6-8
Quench Distance [mm]	0.9	7	1.98
Absolute Minimum Ignition Energy (mJ)	0.02	8	0.1
Specific heat ratio, γ	1.41	1.32	1.535 (vapour)

In prior investigations, researchers typically validated in-cylinder pressure signals for purely hydrocarbon-fuelled engines, often assuming polytropic indices (or coefficients) of around 1.3–1.4 for ideal adiabatic compression [19] . Routine zero-level corrections and dynamic compensation ensured that the measured trace conformed to a polytropic compression and expansion process. Meanwhile, advanced calibration routines or onboard pegging were proposed to maintain absolute data accuracy. To date, limited attention has been paid to ammonia and hydrogen engines, whose dissimilar thermodynamic properties, flame speed characteristics and extended ignition delay may distort polytropic exponents [26, 27]. In such context, referencing well-known polytropic approaches from Brunt et al. [1-4] and from more recent studies [7, 14, 15] with new fuels becomes crucial to avoid significant analysis errors.

The currently reported work addresses the apparent gap by examining the sensitivity of modern in-cylinder pressure measurement routines and conventional analysis techniques when fuelling with ammonia and hydrogen blends. A contemporary Spark Ignition (SI) Single Cylinder Research Engine (SCRE) was employed, featuring variable valve timing, central ignition layout and external boost capability up to 3bar gauge. This engine was of a typical automotive design, with a large data bank of prior in-cylinder pressure data available for different fuels. It was also designed to accommodate direct injection of gasoline alongside dedicated port injection of ammonia or hydrogen. The engine was operated under varied speed, load, and fuel ratios, with spark timing optimised for each condition, targeting maximum brake torque. A Kistler "KiBox2" combustion analysis system was used to collect highspeed in-cylinder and port pressures in real-time. The conventional standard

reverse heat release analysis of the single-zone model was investigated to identify probable error sources in polytropic index mismatch, ignition delay and combustion phasing predictions.

By documenting these offsets and clarifying their impact on advanced fuels, the work helps guide future test procedures and cycle-resolved data-processing routines or hydrogen-ammonia spark ignition combustion engines. In turn, these refinements in cylinder pressure based combustion analysis will be pivotal for enabling robust co-fueling engine control and performance optimisation.

2 EXPERIMENTAL SETUP

Combustion data was obtained using a single-cylinder spark-ignition thermodynamic engine based on the downsized "Di-3" multicylinder variant from MAHLE Powertrain Ltd, with a power density of 120kW/L. Detailed specifications are set out in Table 2. This prototype engine features a pent-roof, Dual Overhead Camshaft (DOHC) cylinder head with fully independent hydraulic intake and exhaust phasers for Variable Valve Timing (VVT) control. The engine has a centrally located spark plug and a side-mounted gasoline direct injector beneath the intake valves, designed for standard gasoline fueling (E10). It is also equipped with separate dedicated port fuel injectors for gaseous ammonia and hydrogen, supplied by Clean Air Power. Ammonia and hydrogen were delivered at purities of 99.5% and 99.97%, respectively. The engine was upgraded with reduced valve lifts and overlaps to minimise unburnt ammonia slip from the combustion chamber. The engine valve timing was kept constant throughout the testing.

Table 2. Engine specification

Parameters	Values
Engine Type	Four Stroke Single Cylinder Spark Ignition
Displaced Volume	400 cc
Bore, Stroke	83 mm, 73.9 mm
Compression Ratio	12.4
Valvetrain	Dual Independent Variable Valve Timing (40°CA Cam Phasing), 4-valve
Fuel Injection Configuration	PFI Hydrogen PFI Ammonia
Cylinder Head Geometry	Pent Roof (High Tumble Port)
Piston Geometry	Pent Roof with cut-outs for valves
Ignition Coil	Single Fire Coil, 100mJ, 30kV
Max Power	40 kW (Gasoline)
Max Torque	96 Nm (Gasoline)
Max In-Cylinder Pressure	120 bar
Max Speed	5000 rpm
Boost System	External boost rig (Max 4barA)
Control System	MAHLE Flexible ECU
Control Software	ETAS INCA

Liquefied ammonia was stored onsite in a commercially supplied drum, with a total capacity of 530 kg at equilibrium vapour pressure. In this initial project phase, port fuel injection (PFI) was selected, extracting gaseous ammonia from above the liquid level in the storage tank. The gaseous ammonia pressure varied between 3 and 4barG, depending on the ambient temperature. Hydrogen was injected similarly, with its pressure staged down in two stages from a Manifold Cylinder Pallet (MCP) at 172barG. The first regulator reduced the pressure to 50 bar to optimise Coriolis flowmeter accuracy (maximum error within 1%), while the second regulator further reduced the pressure to a maximum of 20bar for effective operation of the PFI system. This work package also used a smaller injector to permit optimal injection duration and mitigate the risk of backfire during more extended ignition periods. Safety measures were installed near all injectors, including flashback arrestors and "last-chance" filters. A schematic of the fuel delivery system is shown in Fig 1.

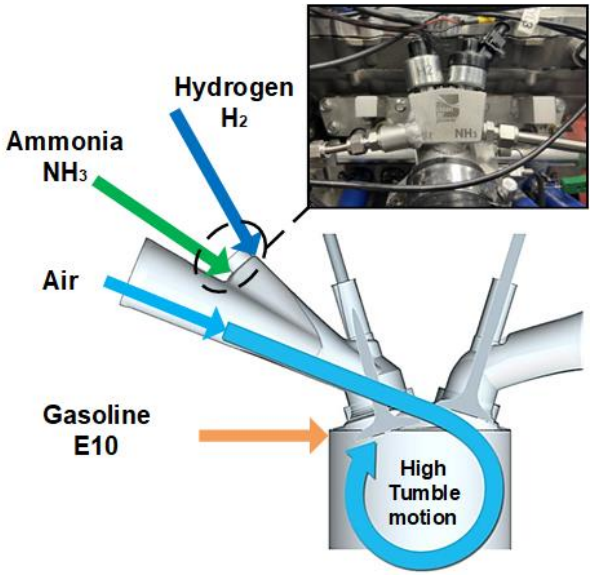

Figure 1. Illustration of engine fuel delivery

The in-cylinder pressure was measured using a Kistler piezoelectric transducer, flush-mounted in the cylinder head. A crank-angle–based pressure method was applied in every recorded cycle. In this approach, referred to as the Intake Manifold Absolute Pressure [15] (IMAPP) [8, 16], the in-cylinder pressure at the Intake Bottom Dead Centre (IBDC) is set equal to the [10] pressure dynamically at the same crank angle for each combustion cycle. As shown in Table 3 are the details of the transducers used, along with the associated uncertainties.

Table 3. Highspeed pressure transducer specifications

Transducer Type	Measuring Location	Model	Range [barA]	Uncertainty (±%FSO)
Piezoelectric	Main Chamber	Kistler 6045B	0…150	<0.2
Piezoresistive	Intake Manifold	Kistler 4045A	0…5	<0.3
	Exhaust Manifold	Kistler 4011A	0…10	<0.1

To ensure the quality of the high-speed engine data, the pressure transducers were calibrated and validated annually using a benchtop hydraulic calibrator with the same measurement chain up to the full-scale range. During testing, a low-pass filter (set at 4kHz) was applied to eliminate high-frequency noises, ensuring consistency across varying levels of hydrogen substitution. Raw pressure data were also recorded and post-processed to verify the accuracy of Mean Effective Pressure (MEP) and heat release calculations.

Daily checkpoints under motoring and at 20% H_2 substitution level under stoichiometric conditions were conducted for data consistency verification (conditions shown in Table 4.). The thermodynamic loss angle variation and the peak in-cylinder pressure were monitored under motoring conditions. At the fired checkpoint, critical fueling settings such as rail pressure, injection angle, throttle opening and spark timing were fixed for each engine hardware configuration. Prior to data logging, the engine was brought to specific target temperature setpoints for coolant, oil, and intake air. Key performance indicators, including Net Indicated Mean Effective Pressure (NMEP), Friction Mean Effective Pressure (FMEP), combustion phasing (CA10, CA50, CA90), combustion stability (coefficient of variation of NMEP, CoV_NIMEP), and gas fuel flow rates (e.g., 20% hydrogen energy basis), were monitored daily. A moving average was calculated for each test run during a 30-second logging period.

Table 4. Daily check points settings (*°aTDCf: crank angle degrees after TDC firing)

Speed	NIMEP [bar]	λ	CA50 [°aTDCf]	Coolant/Oil [°C]	Intake Air [°C]
1400	Motoring	-	-	90	40
1400	10	1.00	8 ±1	90	40

The purpose of this work is to investigate the dependency of the polytropic coefficient on varying hydrogen and ammonia substitution levels, as well as the influence of changing excess air. Additionally, the study evaluates the sensitivity of the conventional single-zone first-law heat release method. This single-zone reverse modelling approach, often employed in industrial combustion analysis equipment, relies primarily on the instantaneous cylinder volume and the measured in-cylinder pressure. It assumes a uniformly distributed air-fuel mixture in the combustion chamber. Accuracy can be improved by adding considerations such as wall heat transfer and blow-by losses.

$$\frac{dQ}{d\theta} = \left(\frac{1}{n-1}\right) * V * \frac{dP}{d\theta} + \left(\frac{n}{n-1}\right) * P * \frac{dV}{d\theta} \quad (1)$$

Equation 1 expresses the rate of heat release in this single-zone first-law model, where:

$dQ/d\theta$	Rate of heat release
n	Polytropic coefficient, as 1.32 assumed globally as gasoline model's default settings
V	Cylinder volume
$dP/d\theta$	Cylinder pressure derivative with respect to (w.r.t.) crank angle
P	Cylinder pressure
$dV/d\theta$	Cylinder volume derivative w.r.t. crank angle

Under adiabatic conditions, where heat transfer is neglected during compression and expansion, the polytropic process is considered reversible (isentropic). Assuming an ideal gas, the polytropic coefficient remains constant and equals the specific heat ratio (γ).

To benchmark and compare with the default heat release calculations for gasoline, an index was determined during the compression and expansion strokes. To avoid noise from pressure waves around valve events and to exclude the rapid changes caused by combustion, a "windowing" approach was used for each stroke. A standard deviation threshold was then applied within that window to dynamically identify a contiguous, stable "flat-line" region rather than relying on fixed valve timing angles. Once the stable portions of the polytropic index trace were identified for compression and expansion strokes, respectively, the crank angle resolved polytropic indices in those regions will be averaged and applied to the heat release calculation.

3 HEAT RELEASE MODEL WITH REVISED POLYTROPIC INDICES FOR PURE AMMONIA COMBUSTION

3.1 Evaluation of Discrepancy of Polytropic Indices and Heat Release Estimation for Conventional First Law Model

This sub-section will cover the evaluation of how polytropic indices vary based on empirical data from pure ammonia combustion under stoichiometric conditions. The first section would provide an initial sensitivity analysis to quantify the deviation from existing gasoline models to the derived indices from testing.

Figure 2 below shows the instantaneous HRR at 1400rpm and 10bar NIMEP (net indicated mean effective pressure) for three scenarios:

Three different first-law heat-release calculation approaches are compared:

1 A fixed global polytropic index of 1.32 (default for gasoline).

2 Fixed indices for compression (1.35) and expansion (1.30), as typically used for gasoline direct injection (DI) models.

3 Cycle-resolved indices derived from high-speed in-cylinder pressure data (pure ammonia combustion in the part load case below).

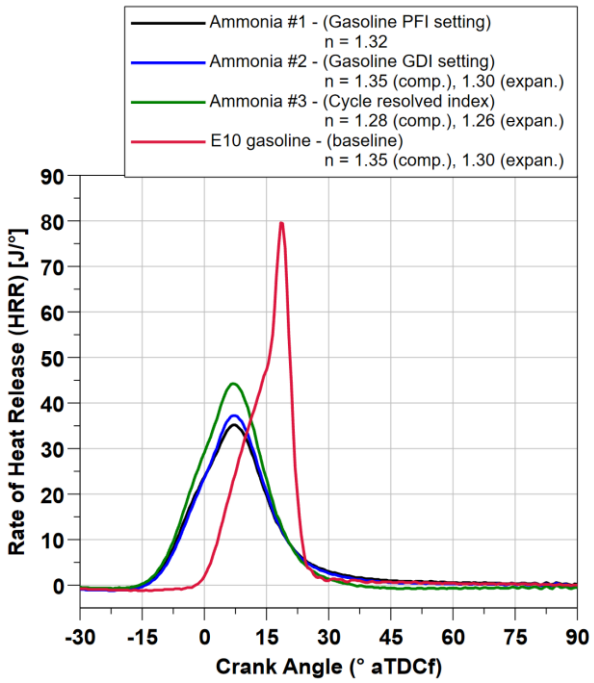

Figure 2. Instantaneous HRR comparison for pure ammonia combustion at 1400rpm/10bar NIMEP

Ammonia exhibits a more distributed heat release rate and thus requires more advanced spark timing compared to gasoline (red line) to achieve the same indicated output. The reduced coefficients (compared to gasoline-based defaults) account for increased heat loss to the cylinder walls, as well as mass transfer effects such as blow-by under real engine conditions. With lower polytropic indices, the denominator in the first-law heat-release equation reduces, causing an earlier, steeper HRR rise before TDC and a higher peak HRR (by approximately 17.5%).

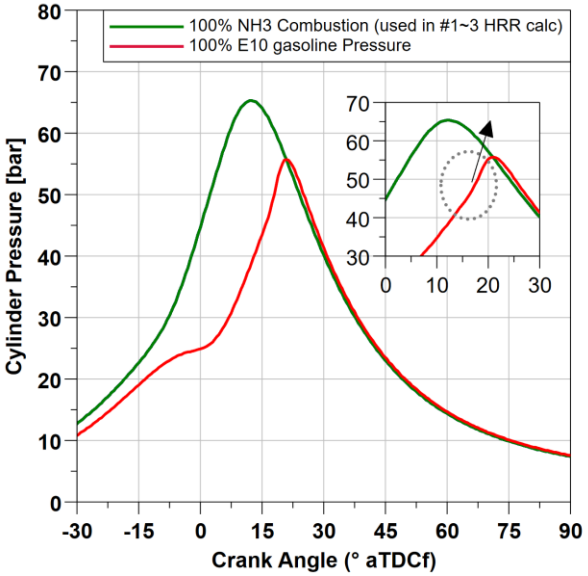

Figure 3. Cylinder pressures for 100% ammonia combustion v.s. 100% gasoline combustion at 1400rpm 10bar NIMEP.

Figure 3 compares the in-cylinder pressure traces for pure ammonia combustion with those obtained from pure gasoline combustion at identical engine speed and load conditions; these pressure data were used to derive the heat release rates previously presented in Fig. 2. For ammonia combustion, the same experimental pressure trace was analysed using three distinct polytropic index methods (#1–3) applied separately during compression and expansion phases, thus illustrating differences in the resulting heat release rates (HRR) and subsequent mass fraction burned calculations. A zoomed-in section of the gasoline combustion pressure trace around TDC firing highlights a notable rapid increase in the rate of pressure rise before reaching peak cylinder pressure, corresponding directly to the previously discussed sharp rise observed in the gasoline HRR curve approximately post 15° aTDCf.

For the benchmarked gasoline operation at this condition, this observed sharp increase can primarily be attributed to significantly retarded spark timing. Specifically, the ignition timing was

intentionally retarded for gasoline operation at this site to maintain the maximum rate of pressure rise (Rmax) below 6 bar/°CA to avoid high knock intensity, adhering to the mechanical limits of the current hardware. This resulted in a substantially delayed combustion phasing, denoted by the CA50, occurring at approximately 16.5° ATDCf, significantly later than the optimal maximum brake torque (MBT) combustion phasing of around 8-10° ATDCf. Under this retarded site, combustion continues to accelerate post-TDC due to persistent high turbulence and elevated temperatures, even though the piston is already descending during expansion. Towards low-speed high-load conditions, gasoline engines typically approach knock-limited operation with necessary retarded timing. In contrast, ammonia exhibits outstanding knock resistance, allowing optimal combustion phasing (CA50) to remain closer to the MBT value of approximately 8° ATDCf, thus better preserving thermal efficiency.

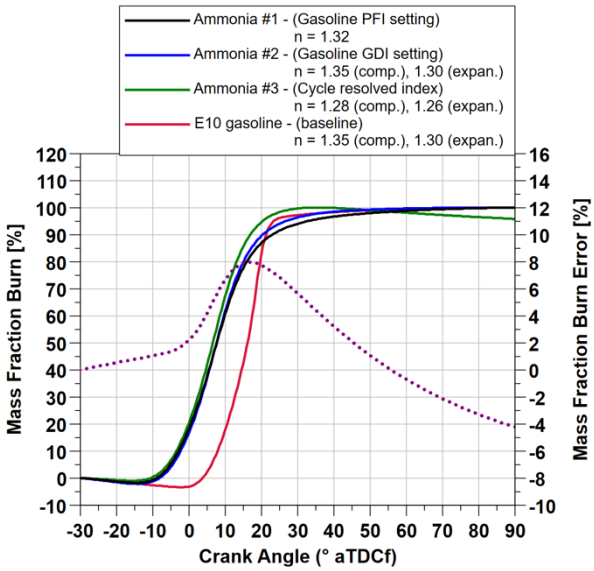

Figure 4. Mass Fraction Burned (MFB) curves at 1400rpm/10bar NIMEP

In Figure 4, the mass fraction burned curves (nominalised cumulative heat release) are shown. A typical calculation window spans from −30° to +90° crank angle around TDC firing, and the maximum value within this window identifies the end of combustion (EOC). The higher polytropic indices used in conventional gasoline models assume smoother heat-release and slower mass-fraction-burned profiles, producing artificially longer combustion durations. With 100% ammonia, the early MFB rise predicted by cycle-resolved indices deviates from these default assumptions. Notably, the default polytropic coefficients remain sufficiently accurate for actual gasoline experiments, whereas ammonia requires more tailored, cycle-resolved values. A difference curve of MFB (purple) helps illustrate how burn rates at specific crank angles diverge, with a maximum error in MFB of 8% at 17° aTDCf, where the revised model indicates 90% fuel mass had been burned, while the default gasoline model predicts only reaching 82%.

3.2 Variation of Polytropic Index with Engine Speed

The purpose of the following subsection is first to evaluate how polytropic coefficients vary by changing engine speeds. The aim was to highlight discrepancies between the indices and the conventional default values for hydrocarbon fuels often used in first-law heat-release models. The high-speed in-cylinder pressure data were gathered from a speed sweep at a constant part-load point where 100% ammonia combustion was sustained. The spark timing was controlled to target maximum brake torque (MBT), ensuring the 50% mass fraction burned (CA50) occurred at ~8° after TDC firing.

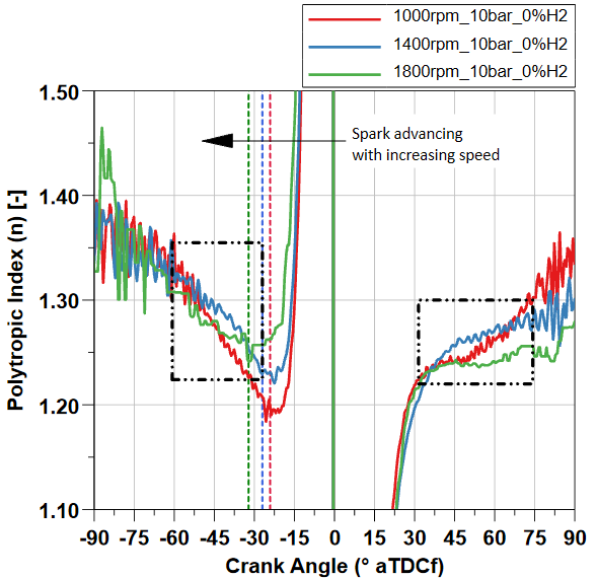

Figure 5. Crank angle resolved polytropic index at constant load (10bar NIMEP)

Figure 5 is the illustration of how the polytropic index evolves in one combustion cycle at three different representative speeds, 1000rpm, 1400rpm, and 1800rpm, zoomed at TDC firing. The index is calculated based on discrete pressure and volume steps between two distinct crank-angle positions from experimental data as Eq. (2).

$$n_i = \frac{\ln\left(\frac{P_i}{P_{i-1}}\right)}{\ln\left(\frac{V_{i-1}}{V_i}\right)} \qquad (2)$$

Although the polytropic exponent curves illustrate general trends over the complete engine cycle, n was explicitly calculated within selected crank-angle windows. These windows were automatically identified in compression and expansion strokes by the analysis algorithm and consisted solely of a continuously stable, noise-free segments (rolling standard deviation < 0.02, size of 5°CA), after intake valve closure (IVC) but before ignition. Example windows were shown in the dashed area in the plot. The result averaged indexes and the windows for calculation are listed in Table 5. Inevitably, the MBT strategy resulted in slight spark-timing variations (spark timing shown as vertical dashed lines, in paired colours) as engine speed increased, typically requiring a 1–2° crank angle advance.

Before combustion started, the index decreased, reached its peak near TDC, and then rapidly dropped as the piston moved down from TDC during the expansion stroke. In non-combustion scenarios, the index would progressively decrease throughout compression until it suddenly peaks at TDC, then again decreases during expansion [28]. In real firing conditions, however, the peak in-cylinder pressure occurs after TDC, which mirrored the polytropic index profile relative to the non-combustion case.

Table 5. Polytropic indexes estimation for compression and expansion strokes at three different speeds (Unit for window °aTDCf)

Speed	Avg. Index Comp./ Expan.	Window Start	Window End
1000rpm	1.253	-59.5	-25
	1.254	24.5	76
1400rpm	1.276	-60.5	-27
	1.255	27.5	72.5
1800rpm	1.274	-52	-37
	1.233	26	77

During compression at lower speeds, the extended cycle duration along with the delayed spark event allowed more time for increased heat transfer from the unburned charge to the cylinder walls, resulting in a lower polytropic index. However, during expansion at 1800 rpm, the polytropic index decreased slightly to an average value of 1.233 compared to around 1.254 and 1.255 at lower speeds. This reduction at higher engine speeds may be attributed to enhanced in-cylinder turbulence and mixing during combustion and early expansion, which can increase heat transfer rates to cylinder walls, thus moderately lowering the observed polytropic index.

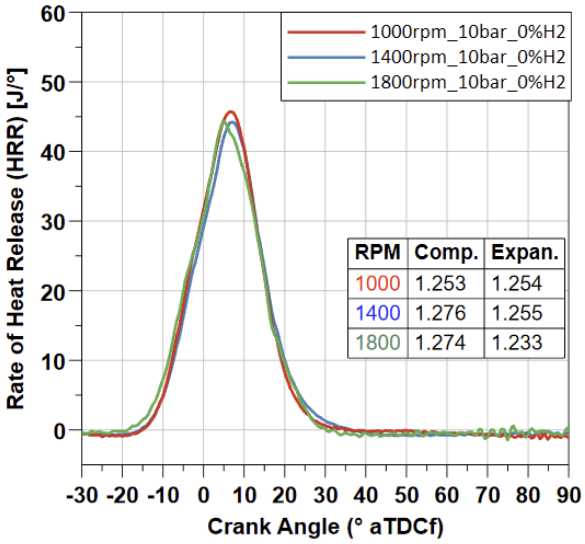

Figure 6. HRR-Constant load speed sweep at 10bar NIMEP

The revised HRR curves with the calculated polytropic indexes for the speed-sweep points are shown in Figure 6 above. It was observed that the instantaneous heat release rates across the three tested engine speeds demonstrated nearly identical profiles when plotted against crank angle. The similarity across different speed conditions may indicate that combustion kinetics and flame propagation at these operating points are primarily governed by in-cylinder flow structures and ignition characteristics rather than engine speed alone. Further diagnostics on a single-cylinder optical engine, as well as a detailed analysis of flame propagation speed, turbulence intensity, and combustion timing, could help substantiate the mechanisms responsible for this convergence in heat release behaviour.

Table 6. Burn durations comparison at different engine speeds for pure ammonia combustion

Speed	Spark Tmg. [°aTDCf]	Ign. Delay [°]	CA50 [°aTDCf]	CA10-90 or BD [°]
1000rpm	-24.9	21.3	6.1	19.4
1400rpm	-27.2	23.8	6.6	20.4
1800rpm	-36.8	31.9	5.6	20.9

Table 6 also summarises key combustion metrics, including ignition delay (spark to CA10), combustion phasing (CA50), and burn duration (CA10–90). It should be noted that during the original testing, a constant polytropic coefficient (n = 1.32) was applied for indicated analysis, hence the revised heat release calculation with cycle-resolved indexes yields slightly advanced CA50 at around 6° aTDCf.

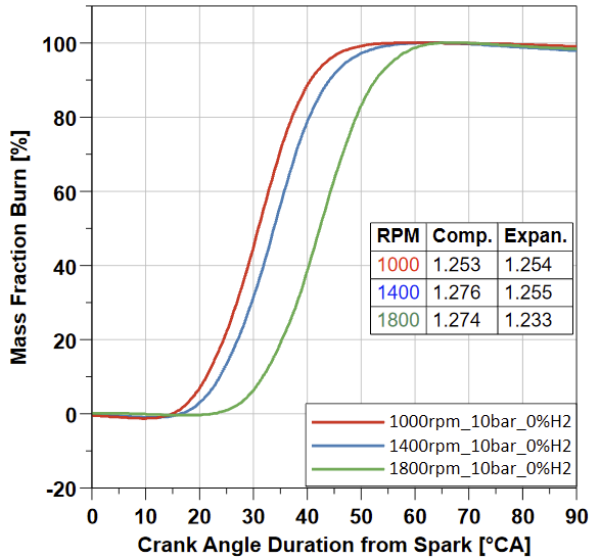

Figure 7. MFB and durations for constant load speed sweep at 10bar NIMEP

To explore the effect of necessary spark advancement implemented in the speed sweeps, the MFB curves were realigned relative to their respective spark events, as presented in Figure 7. In this plot, the horizontal axis represents the crank angle degrees after the spark events. It can be observed that the ignition delay becomes more pronounced at higher engine speeds, thereby requiring more significant spark advancement to achieve consistent combustion phasing (CA50).

4 INFLUENCE OF HYDROGEN SUBSTITUTION AND EXCESS AIR RATIO

4.1 Impact of hydrogen addition and excess air on polytropic index

The work presented in this chapter investigates the thermodynamic sensitivity of ammonia-hydrogen fuel blends and the effects of varying the excess air ratio, specifically for the lean-burn combustion strategy previously proposed for ammonia-hydrogen co-firing [29]. The cycle-resolved averaging method for calculating the polytropic exponent was selected explicitly to evaluate its sensitivity to fuel composition and operating conditions.

Figure 8 shows polytropic indices around TDC firing for various hydrogen substitution levels (0–60%) in the ammonia fuel blend at 1400rpm and 6bar NIMEP. Hydrogen's higher laminar burning velocity reduces the need for spark advance, resulting in an even lower polytropic index prior to combustion. Despite the varying hydrogen content, there is a strong agreement of the initial part of the polytropic index traces before combustion was initiated. However, for higher hydrogen substitution level blends, the index continues to drop during the compression stroke, as delayed spark timing allows more heat transfer temporally and lowers the in-cylinder temperature.

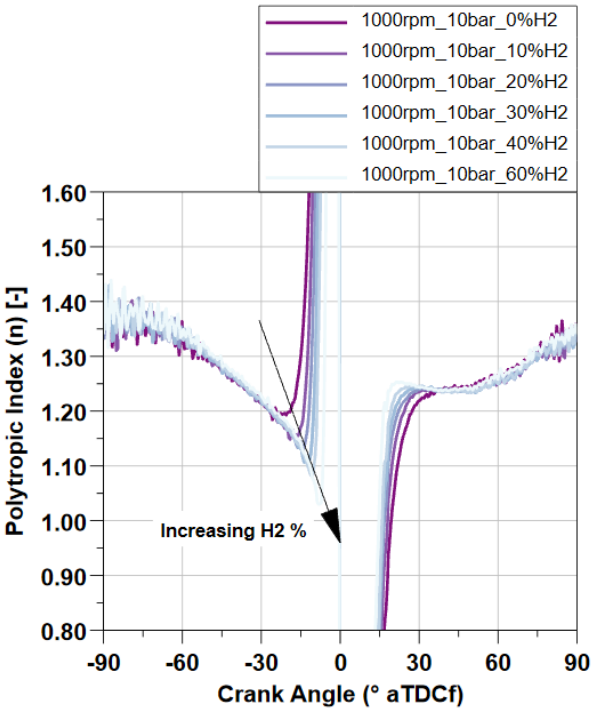

Figure 8. Polytropic index variation with different hydrogen substitution levels

Although an averaging window technique for polytropic indices can be implemented in real-time, a more nuanced correction mapping polytropic index to the specific heat ratio (γ) as a function of crank angle would improve accuracy in stepwise heat-release calculations [1].

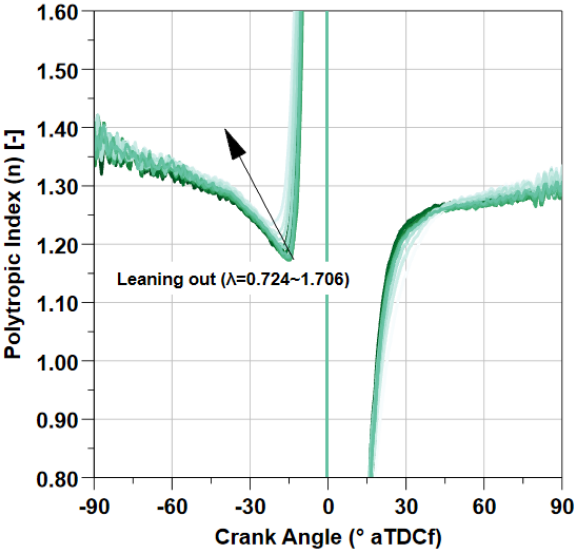

Figure 9. Polytropic index variation with increasing level of excess air ratio λ

A variation trend is also shown for the polytropic index for a lambda sweep at fixed 20% energy-

based hydrogen in Figure 9. The darker colour denoted a richer mixture. When sweeping from rich to near stoichiometric conditions (λ ≈ 0.724 to 1.007), less excess fuel remains to absorb heat. Consequently, average in-cylinder temperatures increase, resulting in shorter burn durations, observable by the steeper HRR curve at higher lambda in Figure 10 below. However, as the mixture becomes leaner beyond λ = 1.007 up to λ = 1.726, the increased excess air lowers the peak combustion temperature and slows the burn, eventually reaching a combustion stability limit at 3% CoV of NIMEP with 20% hydrogen substitution.

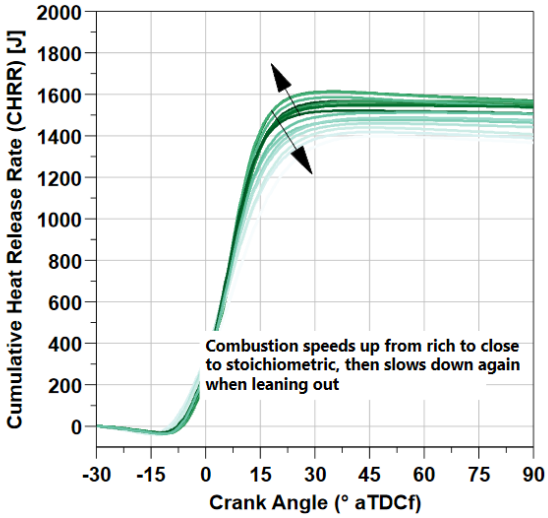

Figure 10. CHRR for 20% hydrogen, lambda sweeps at 1400, 10bar (0.724~1.706)

4.2 Sensitivity of Lambda and hydrogen-ammonia substitution level on heat release calculation

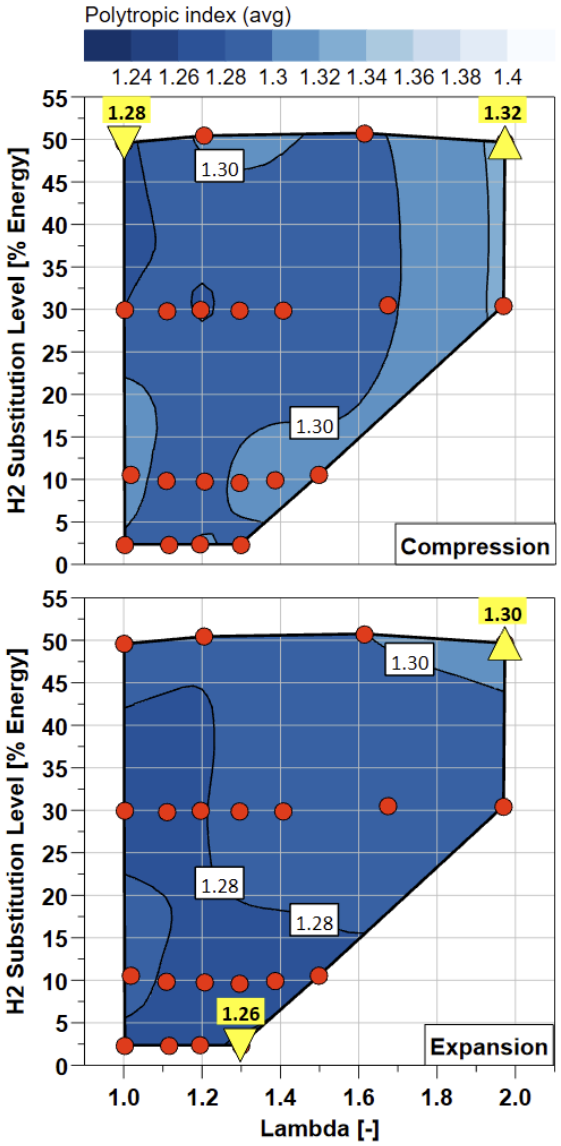

Figure 11. Averaged polytropic index variations for compression (upper) and expansion (lower) stroke in hydrogen and lambda mapping (Yellow triangles indicated minimum (down) and maximum (up)

Illustrated in Figure 11 is an example of how the polytropic indices for compression and expansion vary with hydrogen substitution and lambda at 1400rpm and a low load condition of 6bar NIMEP. Each red dot in the 3-D plot indicates an assessed test point. The yellow triangles show the minimum (downward) and maximum (upward) values. The overall span in each index is around 0.04, regardless of the hydrogen substitution ratio, implying limited dependence on hydrogen and lambda at this operating site. Consequently, adopting a constant index or mapping a small range of values may be feasible based primarily on speed and load. The difference between the

averaged expansion and compression indices also remains minor, reaching approximately 0.04 under lower hydrogen substitution.

The combustion duration was compared between the original constant index method from gasoline (1.32 for stoichiometric gasoline combustion) and the improved 1st law with revised n from cyclic data. Shown in Figures 12-14 are the burn duration results with default gasoline settings (upper plot), against the improved 1st law method with revised indices (lower plot). Figure 11 shows the early burn stage, which was marked by the first 50% mass fraction burned point. The heat release rates in the two methods show similar trends and spans, with only slight differences at low hydrogen substitution levels towards the lean limit conditions.

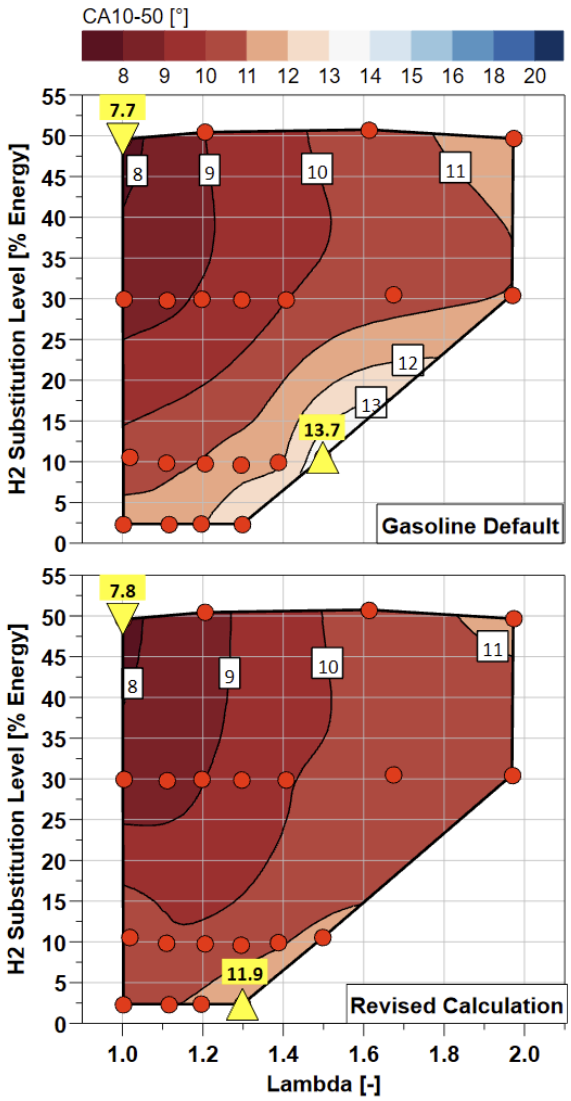

Figure 12. Early-stage combustion duration (CA10-50) comparison for the gasoline default setting upper), and revised indices (lower)

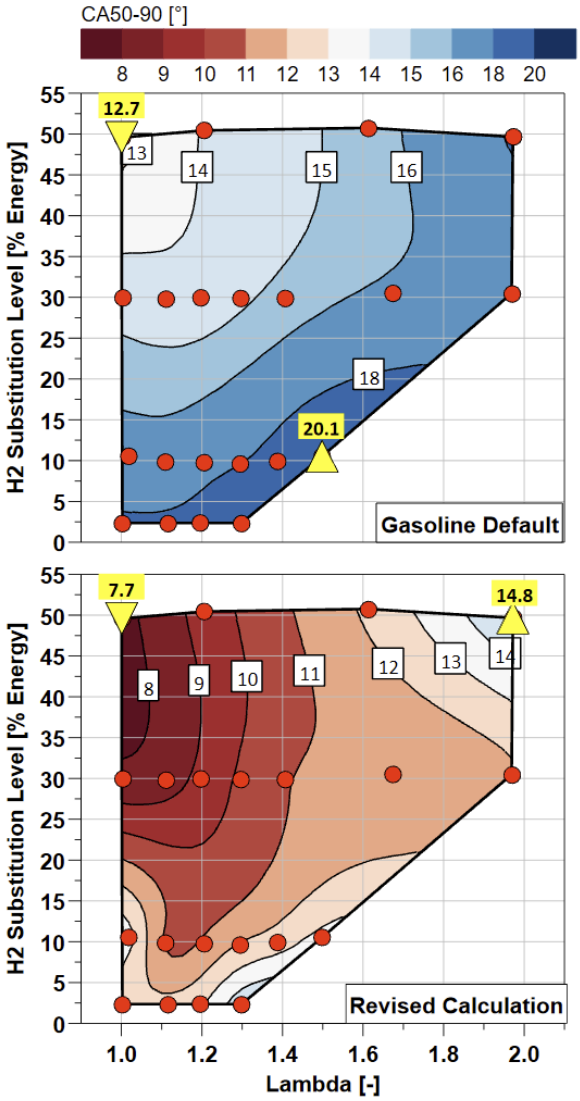

Figure 13. Late-stage combustion duration (CA50-90) comparison for the gasoline default setting upper), and revised indices (lower)

Figure 13 shows the late burning phase, denoted by CA50-90. A reduction was seen on both plots with higher hydrogen content and less excess air added. The span of late burn duration for gasoline settings varied from 13-20 degrees, whilst the revised calculation showed a reduction of the span with only 8-15 degrees. Figure 14 at the end represents the total duration. The dark colour in the revised calculation in the lower map indicated an overall reduction.

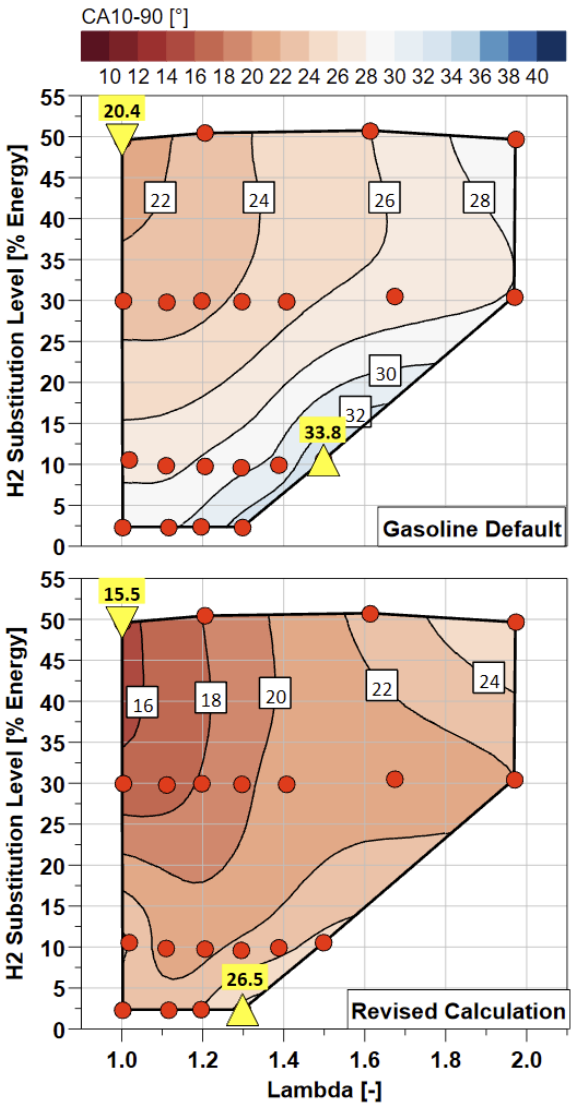

Figure 14. Overall combustion durations (CA10-90) comparison for the gasoline default setting upper), and revised indices (lower)

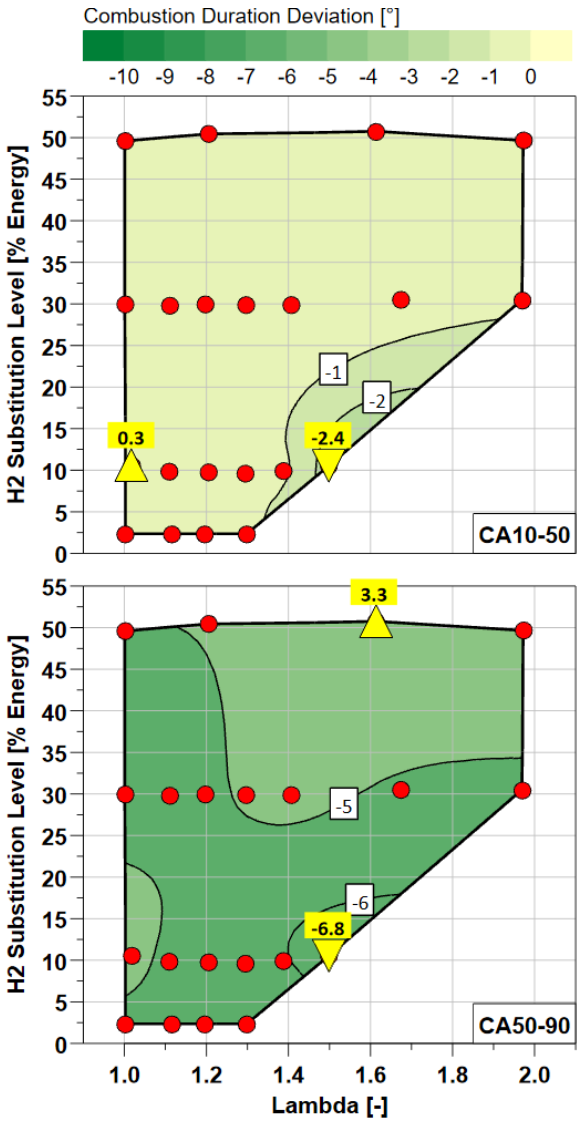

Figure 15. Burn duration deviation using revised polytropic indices(negative values for reduction)

To quantify the deviation introduced using the default gasoline polytropic index, two difference maps are shown in Figure 15, illustrating deviations during the early burn stage (upper: 10–50% fuel mass burned) and the late burn stage (lower: 50–90%). These maps highlight the reductions required to correct predictions based on the gasoline model. The maximum deviation during the early burn stage is approximately 2 degrees advancement, observed under low hydrogen substitution conditions near the lean stability limit. Such discrepancies could lead to moderate inaccurate spark timing control and mispredictions of combustion phasing. The trend indicates a gradual decrease in calculation difference as the hydrogen content in the fuel mix increases, with the deviation further diminishing closer to stoichiometric conditions.

In contrast, the late burn duration (50–90%) shows a significant error, ranging from 3 to 7 degrees of reduction when the revised indices were applied. Comparing the two maps reveals that the primary source of burn duration calculation error lies in the second half of the combustion process or the late-burn stage. This suggests that the default indices of 1.32 for gasoline operations would result in more significant errors when predicting the end of combustion.

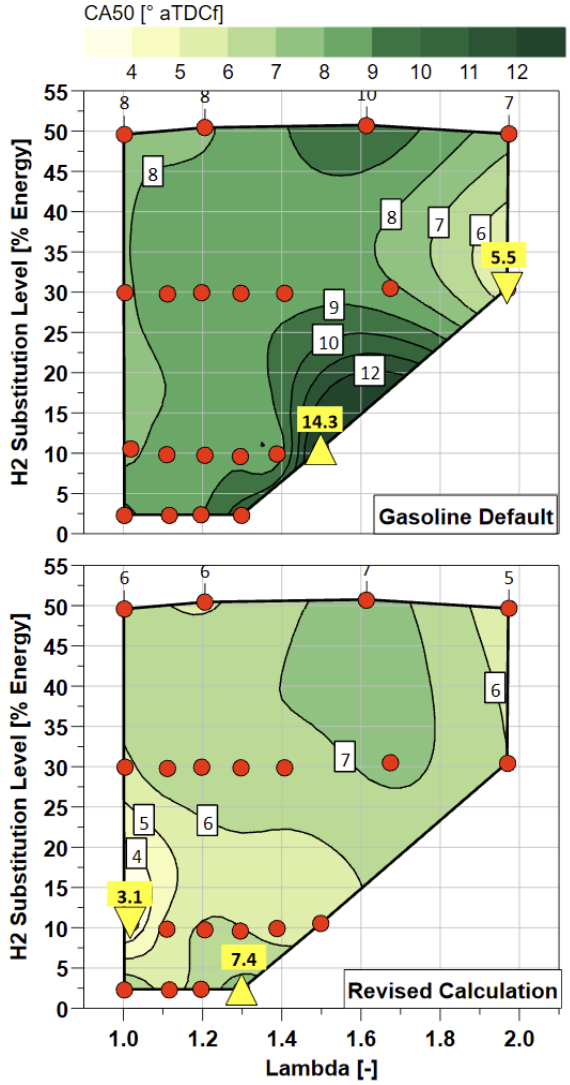

Figure 16. Combustion phasing at 50% mass fraction burn for the gasoline default setting upper) and revise indices (lower)

In conventional spark-ignited engines, the CA50 timing is typically around 8-10 degrees after TDC. Figure 16 shows the position of CA50 at this part load condition. As the mixture was leaned out, flame propagation slowed, and as a result, the CA50 progressively shifted beyond this nominal MBT window, regardless of further spark advance. This is however less evident as hydrogen started to dominate the fuel mix. In contrast, the adjusted calculation using revised indices can predict a faster heat release rate and then return the modelled CA50 closer to the typical MBT location.

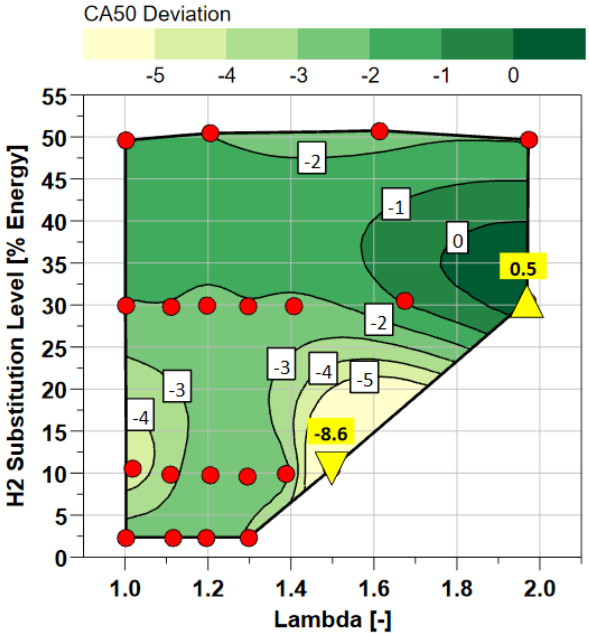

Figure 17. Combustion phasing deviation with 1st Law calculation using gasoline default indices (negative values for advancement)

The difference map is shown as the deviation for combustion phasing prediction in Figure 17 from the two methods. As predicted in the 10-50% MFB profiles, the revised indices produced an earlier 50% burn location. The default 1st Law calculation could result in a maximum error of 9 degrees under actual lean-limit conditions.

Further analysis focused on the ignition delay, representing the initial flame kernel formation and early flame front growth. In Figure 18, the lower plot illustrates spark timing to achieve maximum brake torque, showing a reduced requirement for spark advancement as the hydrogen percentage increased and the excess air ratio was reduced. These changes raised the average combustion temperature, thereby shortening the ignition delay. At the other extreme, when leaning out under high ammonia fuel mix ratios (diagonally towards the bottom right corner), the ignition delay period expands as it approaches the combustion stability limit. Shown in the error plot in Figure 19 in negative magnitudes demonstrated a negligible reduction of a maximum of 1.3 crank angle degrees in ignition delay with the revised model. This trend was consistent across the entire range of the mapping regardless of fuel substitution and excess air levels.

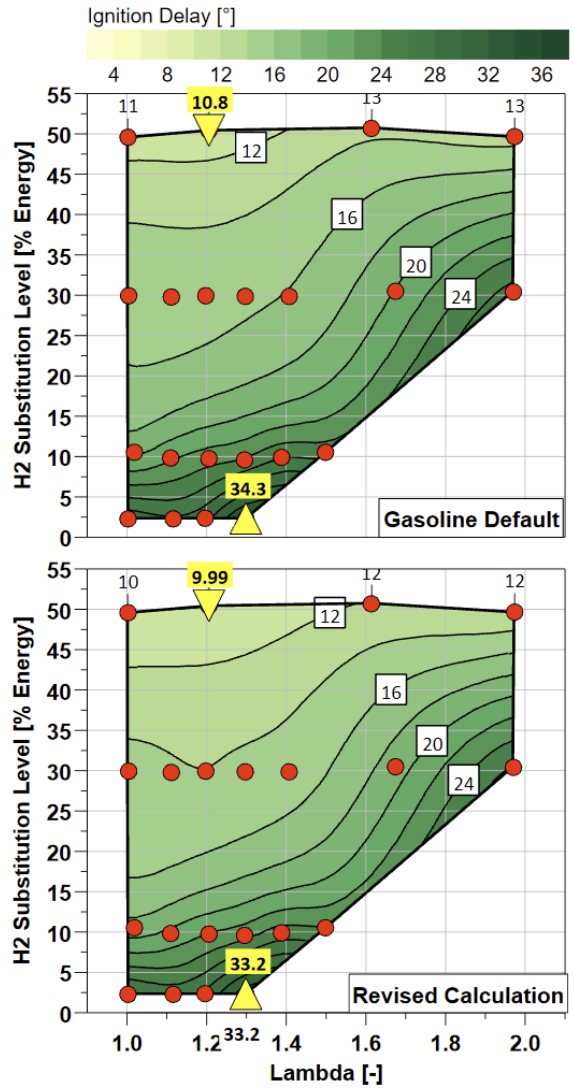

Figure 18. Ignition delay calculation comparison for the gasoline default setting upper) and revised indices (lower)

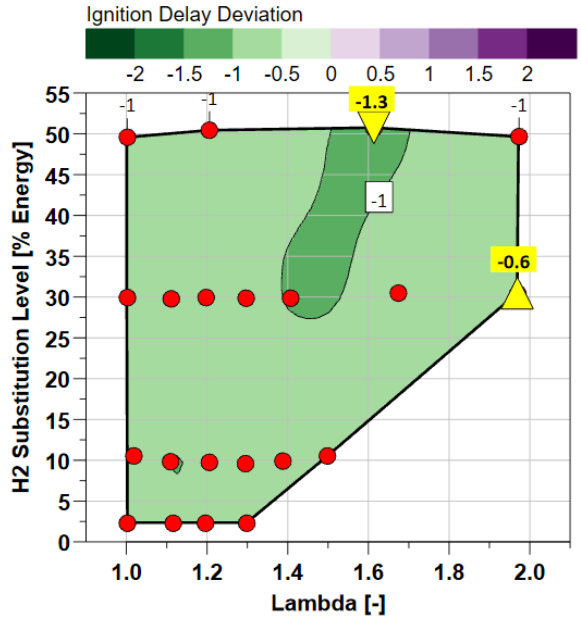

Figure 19 Ignition delay calculation deviation

5 CONCLUSIONS

The currently reported work has demonstrated that ammonia–hydrogen co-combustion exhibits notably distinct heat release profiles compared to conventional fossil-fuel operation, largely due to ammonia's unique thermodynamic properties. The results were obtained in an automotive engine, but the findings should be applicable across four-stroke spark ignition operations using equivalent fuelling systems. Overall, the work has proven that bespoke combustion analysis metrics are required for such ammonia and hydrogen engine operation to ensure adequately precise measurements are obtained and avoid delays and increased costs during engine development.

When applying a conventional First Law reverse mode heat-release analysis, it was found that polytropic indices must be carefully revised to maintain accuracy in predicting combustion duration and phasing. In particular, a conventional gasoline-based stoichiometric combustion model can shift the polytropic index, n, in compression by up to 3.7% and in expansion by 3.9% under 100% ammonia fuelling. Incorporating crank-angle-resolved polytropic indices derived from in-cylinder pressure data significantly improved the fidelity of the heat-release calculations.

Fuel substitution and relative air-to-fuel ratio sweep at 1400rpm, 10bar NIMEP, suggesting that it may be feasible to employ a single cycle coefficient in scenarios where ammonia dominates the overall fuel blend. While gasoline lean-burn (GDI) can tolerate higher hydrogen mixes (1.38 for compression and 1.30 for expansion) using existing indices 1.32, respectively, ammonia's lower specific heat ratio and slower flame speed produced distinct heat-release characteristics, thereby necessitating a revised modelling approach.

- Under medium speed and load conditions (1400rpm, 10bar NIMEP), the maximum variance in polytropic indices was approximately 0.04 (for both compression and expansion).

- When hydrogen content was increased up to a 50/50 ratio with ammonia, accompanied by excess air up to the lean stability limit, the reduction in late-stage combustion (CA50–90) of about 7°CA suggested by the revised HHR, translated to a substantial 35% decrease in burn duration. This indicates a possible delayed EOC estimation when utilising a high polytropic index for ammonia combustion, as the cumulative heat release curve may still be

incomplete after the real combustion event has been physically completed.

- By contrast, the initial burn phase (CA0–50) was reduced by only 2°CA (14%), indicating that hydrogen and additional air predominantly influence the latter combustion stage. Despite these variations, combustion phasing varied by only about 2°CA overall, suggesting that spark-timing control for MBT strategies remains manageable.

- Furthermore, ignition delay, modelled using both a standard gasoline approach and an improved First Law method, showed close agreement with deviations within 1°CA across the operating range tested.

Future work will be followed below to validate the sensitivity at broader speed-load operating conditions as follows.

1 Extended Operating Map

Investigate hydrogen–ammonia substitution at broader speeds (1,000–4,000 rpm) and loads (up to 30 bar NIMEP) to validate further how the substitution level and lambda affect polytropic indices.

2 Non-combustion (motoring) Compression Testing

Perform dedicated compression tests (no combustion) across a mini speed–load map to correlate measured polytropic coefficients more directly with the ratio of specific heats (γ). These data can refine crank-angle–step calculations for the heat release rate.

3 Spark-Timing Sweeps

Conduct systematic spark-timing sweeps to pinpoint MBT phasing with ammonia–hydrogen blends. This will help confirm whether the CA50 target of ~8° aTDCf remains optimal under varied fuel compositions and operating conditions.

4 Real-time implementation in Kistler Kibox2 combustion analysis system

In comparison with previous studies, this updated polytropic index calculation method can be used to determine the index on a cycle-by-cycle basis to help compensate for cyclic variations. This enables more precise combustion phasing control and provides operators with enhanced accuracy in engine control for complex alternative fuel blends and premixed modes. This enhanced approach will be incorporated into the combustion analysis platform for validation on a 170 mm bore flex-fuel SCRE, enabling correlation with ongoing ammonia–hydrogen combustion modelling at the University of Nottingham.

6 DEFINITIONS, ACRONYMS, ABBREVIATIONS

aTDCf: After Top Dead Centre Firing

BD: Burn (Combustion) Duration

CA: Crank Angle

CHRR: Cumulative Heat Release Rate

CoV: Coefficient of Variance

DI: Direct Injection

HRR: Heat Release Rate (instantaneous)

IMAPP: Intake Manifold Absolute Pressure Pegging

MFB: Mass Fraction Burnt

NIMEP: Net Indicated Mean Effective Pressure

SI: Spark Ignition

TDC: Top Dead Centre

VVT: Variable Valve Timing

7 ACKNOWLEDGEMENTS

The authors would like to acknowledge the support of the UK EPSRC in co-funding this research through the MariNH_3 (Grant Ref# EP/W016656/1) and the UK Clean Maritime Research Hub (Grant Ref# EP/Y024605/1) research programmes.

8 REFERENCES AND BIBLIOGRAPHY

1. Brunt, M.F.J. and K.C. Platts, *Calculation of Heat Release in Direct Injection Diesel Engines*. 1999, SAE International.

2. Brunt, M.F.J., H. Rai, and A.L. Emtage, *The Calculation of Heat Release Energy from Engine Cylinder Pressure Data*. 1998, SAE International.

3. Brunt, M.F.J. and C.R. Pond, *Evaluation of Techniques for Absolute Cylinder Pressure Correction*. 1997, SAE International.

4. Brunt, M.F.J. and A.L. Emtage, *Evaluation of Burn Rate Routines and Analysis Errors*. 1997, SAE International.

5. Davis, R.S. and G.J. Patterson, *Cylinder Pressure Data Quality Checks and*

Procedures to Maximize Data Accuracy. 2006, SAE International.

6. Patterson, G.J. and R.S. Davis, *Geometric and Topological Considerations to Maximize Remotely Mounted Cylinder Pressure Transducer Data Quality.* SAE International Journal of Engines, 2009. **2**(1): p. 414-420.
7. Rogers, D.R., A. Pezouvanis, and N. Kalantzis, *A Model-based Method of Monitoring Combustion Pressure Measurement Chains for Closed-loop Combustion Control Applications.* American Journal of Mechanical Engineering, 2021. **9**(1): p. 24-40.
8. Randolph, A.L., *Methods of Processing Cylinder-Pressure Transducer Signals to Maximize Data Accuracy*. 1990, SAE International.
9. Randolph, A.L., *Cylinder-Pressure-Transducer Mounting Techniques to Maximize Data Accuracy*. 1990, SAE International.
10. Randolph, A.L., *Cylinder-Pressure-Based Combustion Analysis in Race Engines*. 1994, SAE International.
11. Amann, C.A., *Cylinder-Pressure measurement and Its Use in Engine Research*. 1985, SAE International.
12. Amann, C.A., *Classical Combustion Diagnostics for Engine Research*. 1985, SAE International.
13. Soltis, D.A., *Evaluation of Cylinder Pressure Transducer Accuracy based upon Mounting Style, Heat Shields, and Watercooling*. 2005, SAE International.
14. Balmelli, M., et al., *Method for pressure trace based thermodynamic analysis of pre-chamber combustion.* Energy Conversion and Management, 2024. **312**: p. 118561.
15. Nahkle, M., et al., *A Method for Improvement in Data Quality of Heat Release Metrics Utilizing Dynamic Calculation of Cylinder Compression Ratio.* SAE International Journal of Engines, 2019. **13**(2): p. 135-142.
16. Rogers, D.R., *Engine Combustion: Pressure Measurement and Analysis*. 2010: SAE International.
17. Ambalakatte, A., et al., *Evaluation of ammonia-gasoline co-combustion in a modern spark ignition research engine.* Carbon Neutrality, 2023. **2**(1): p. 35.
18. Ambalakatte, A., et al., *Evaluation of Ammonia Co-fuelling in Modern Four Stroke Engines.* Johnson Matthey Technology Review, 2023.
19. Luo, Q.-h., B.-g. Sun, and H.-y. Tian, *The characteristic of polytropic coefficient of compression stroke in hydrogen internal combustion engine.* International Journal of Hydrogen Energy, 2014. **39**(25): p. 13787-13792.
20. Ulucan, T.H., et al., *Hydrogen storage in liquid hydrogen carriers: recent activities and new trends.* Progress in Energy, 2023. **5**(1): p. 012004.
21. J. R. GROVE. *THE MEASUREMENT OF QUENCHING DIAMETERS AND THEIR RELATION TO THE FLAMEPROOF GROUPING OF GASES AND VAPOURS*. in *I.Chem.E. SYMPOSIUM SERIES No. 25*. 1968. London, UK: Institution of Chemical Engineers (I.Chem.E).
22. Dimitriou, P. and R. Javaid, *A review of ammonia as a compression ignition engine fuel.* International Journal of Hydrogen Energy, 2020. **45**(11): p. 7098-7118.
23. Lhuillier, C., et al., *Combustion Characteristics of Ammonia in a Modern Spark-Ignition Engine*. 2019, SAE International.
24. Kumamoto, A., et al., *Measurement of minimum ignition energy in hydrogen-oxygen-nitrogen premixed gas by spark discharge.* Journal of Physics: Conference Series, 2011. **301**(1): p. 012039.
25. Ciniviz, M. and H. Köse. *HYDROGEN USE IN INTERNAL COMBUSTION ENGINE: A REVIEW*. 2012.
26. Kuratle, R.H. and B. Märki, *Influencing Parameters and Error Sources During Indication on Internal Combustion Engines*. 1992, SAE International.
27. Puzinauskas, P.V., W.M. Mathis, and M.A. Dzieciuch, *Quantification and Modeling the Effects of Thermal Shock on Combustion Pressure Transducers*. 2001, SAE International.
28. Brunt, M.F.J., C.R. Pond, and J. Biundo, *Gasoline Engine Knock Analysis using Cylinder Pressure Data*. 1998, SAE International.
29. Geng, S., A. Ambalakatte, and A. Cairns. *Ammonia and Hydrogen Co-Fuelling in a Modern Spark Ignition Engine*. in *MariNH3 Annual Conference*. 2024. Nottingham: MariNH3.